Fitted Finite Element Discretization of Two–Phase Stokes Flow

Marco Agnese and Robert Nürnberg*
Department of Mathematics, Imperial College, London, SW7 2AZ, U.K.

Abstract

We propose a novel fitted finite element method for two-phase Stokes flow problems that uses piecewise linear finite elements to approximate the moving interface. The method can be shown to be unconditionally stable. Moreover, spherical stationary solutions are captured exactly by the numerical approximation. In addition, the meshes describing the discrete interface in general do not deteriorate in time, which means that in numerical simulations a smoothing or a remeshing of the interface mesh is not necessary. We present several numerical experiments for our numerical method, which demonstrate the accuracy and robustness of the proposed algorithm.

Key words. viscous incompressible two-phase flow, Stokes equations, free boundary problem, surface tension, finite elements, front tracking

1 Introduction

Fluid flow problems with a moving interface are encountered in many applications in physics, engineering and biophysics. Developing robust and efficient numerical methods for these flows is an important problem and has attracted tremendous interest over the last decade. Apart from the usual difficulties arising from the numerical computation of the fluid flow in the bulk, the accurate approximation of the moving free interface, as well as a suitable description of the conditions that need to hold on the interface, pose serious challenges. Of particular importance is the precise inclusion of surface tension terms, and the correct handling of discontinuity jumps in the material properties and in the pressure at the interface, in order to suppress spurious velocities, which are also called parasitic currents.

*email: {m.agnese13,robert.nurnberg}@imperial.ac.uk

In this paper we propose a novel finite element approximation for incompressible two-phase Stokes flow that naturally avoids spurious velocities. Our scheme is based on the numerical method introduced in [7], and so uses piecewise linear parametric finite elements to describe the moving discrete interface. In contrast to [7], where the interface and the bulk mesh were totally independent, here we pursue the fitted approach. That means that the interface discretization is always fitted to the bulk mesh, i.e. the discrete interface is made up of edges/faces of elements belonging to the bulk mesh. An advantage of our method is that the discontinuity jumps in the material properties and in the pressure are captured naturally. In particular, we do not need to employ an XFEM-type extension of standard bulk pressure spaces. Surface tension forces are discretized with the help of a variational approximation of curvature that was first proposed in [4, 5]. Combining this with an implicit treatment of the surface tension forces yields an unconditionally stable scheme. Interestingly, the formulation of curvature from [4] leads to a tangential motion of vertices in practice, which guarantees equidistribution in 2d and good meshes in 3d. Overall, our proposed method has the following properties.

- The fully discrete scheme is unconditionally stable in the sense that the total surface energy is monotonically decreasing independent of the chosen time step size.

- In the absence of outer forces, any discrete solution with a stationary interface must have zero velocity globally, i.e. we can prove that there are no stationary solutions with spurious velocities. Similarly, discrete stationary solutions for spherical interfaces are attained for our scheme.

- For the semidiscrete continuous-in-time variant of the fully discrete scheme the volume of the two phases is conserved. The fully discrete scheme itself maintains the enclosed volumes well in practice.

- Thanks to the fitted nature of the finite element method, the pressure jumps at the interface are captured accurately for standard pressure finite element spaces without the need for XFEM extensions.

- The surface tension effects are included with the help of a variational treatment of curvature based on the Laplace–Beltrami operator.

- The surface mesh quality is maintained. In particular, for the semidiscrete scheme an equidistribution property can be shown in 2d.

- The fully discrete scheme uses an implicit approximation of curvature that leads to a coupled linear system of equations to be solved at each time step.

Let us briefly discuss alternative approaches to the numerical approximation of two-phase flow problems. In this paper we use a direct description of the interface. In such direct approaches, which are often called front-tracking methods, the interface is either triangulated or presented by a connected set of particles. The discrete interface is advected with the help of the bulk fluid velocities, and quantities on the interface need to be suitably coupled to the bulk equations. In our situation, a finite element parameterization of the unknown interface is employed. We refer e.g. to [37, 3, 36, 18, 19, 7] for further details on front tracking methods, and to [27, 30] for the related immersed boundary method. Another class of approaches is based on interface capturing methods using an indicator function to describe the interface. The volume of fluid (VOF) method and the level set method fall into this category. In the former, the characteristic function of one of the phases is approximated numerically, see e.g. [24, 32, 31]; whereas in the latter, the interface is given as the level set of a function, which has to be determined, see e.g. [35, 34, 29, 22]. Finally, in phase field methods the interface is assumed to have a small, but positive, thickness and an additional parabolic equation, defined in the whole domain, has to be solved in these so-called diffuse interface models. We refer to [25, 2, 28, 16, 26, 1, 23] for details.

The remainder of this paper is organized as follows. In Section 2 we present the mathematical model and the weak formulation on which our finite element approximation is going to be based. Our numerical method is presented in Section 3, together with proofs for its main properties. In addition, we describe how the arising linear systems of equations are solved in practice, and we give details on our mesh generation and smoothing procedures. Finally, in Section 4 we present several numerical simulations in 2d and 3d.

2 Mathematical model

2.1 Governing equations

In this paper we consider two-phase Stokes flow in a given domain $\Omega \subset \mathbb{R}^d$, where $d = 2$ or $d = 3$. The domain Ω contains two different immiscible, incompressible, viscous fluids (liquid-liquid or liquid-gas) which for all $t \in [0, T]$ occupy time dependent regions $\Omega_+(t)$ and $\Omega_-(t) := \Omega \setminus \overline{\Omega}_+(t)$ and which are separated by an interface $(\Gamma(t))_{t\in[0,T]}$, $\Gamma(t) \subset \Omega$. See Figure 1 for an illustration. For later use, we assume that $(\Gamma(t))_{t\in[0,T]}$ is a sufficiently smooth evolving hypersurface without boundary that is parameterized by $\vec{x}(\cdot, t) : \Upsilon \to \mathbb{R}^d$, where $\Upsilon \subset \mathbb{R}^d$ is a given reference manifold, i.e. $\Gamma(t) = \vec{x}(\Upsilon, t)$. Then

$$\vec{\mathcal{V}}(\vec{z}, t) := \vec{x}_t(\vec{q}, t) \qquad \forall\ \vec{z} = \vec{x}(\vec{q}, t) \in \Gamma(t) \tag{2.1}$$

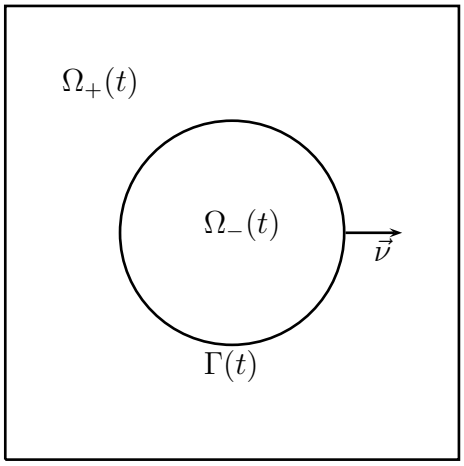

Figure 1: The domain Ω in the case $d = 2$.

defines the velocity of $\Gamma(t)$, and $\vec{\mathcal{V}} \,.\, \vec{\nu}$ is the normal velocity of the evolving hypersurface $\Gamma(t)$, where $\vec{\nu}(t)$ is the unit normal on $\Gamma(t)$ pointing into $\Omega_+(t)$.

Denoting the velocity and pressure by $\vec{u}$ and p, respectively, we introduce the stress tensor

$$\underline{\underline{\sigma}} = \mu \,(\nabla \,\vec{u} + (\nabla \,\vec{u})^T) - p\,\underline{\underline{\mathrm{id}}} = 2\,\mu\,\underline{\underline{D}}(\vec{u}) - p\,\underline{\underline{\mathrm{id}}}\,, \tag{2.2}$$

where $\mu(t) = \mu_+\,\mathcal{X}_{\Omega_+(t)} + \mu_-\,\mathcal{X}_{\Omega_-(t)}$, with $\mu_\pm \in \mathbb{R}_{>0}$, denotes the dynamic viscosities in the two phases, $\underline{\underline{\mathrm{id}}} \in \mathbb{R}^{d\times d}$ is the identity matrix and $\underline{\underline{D}}(\vec{u}) := \frac{1}{2}\,(\nabla\vec{u} + (\nabla\vec{u})^T)$ is the rate-of-deformation tensor.

In this paper we consider a two-phase Stokes problem, and so the equations governing the fluid are

$$-\nabla \,.\, \underline{\underline{\sigma}} = \vec{f} \qquad \text{in } \Omega_\pm(t)\,, \tag{2.3a}$$
$$\nabla \,.\, \vec{u} = 0 \qquad \text{in } \Omega_\pm(t)\,, \tag{2.3b}$$

where $\vec{f}$ is a possible forcing term.

On the free surface $\Gamma(t)$, the following conditions need to hold:

$$[\vec{u}]^+_- = \vec{0} \qquad \text{on } \Gamma(t)\,, \tag{2.4a}$$
$$[\underline{\underline{\sigma}}\,\vec{\nu}]^+_- = -\gamma\,\varkappa\,\vec{\nu} \qquad \text{on } \Gamma(t)\,, \tag{2.4b}$$
$$\vec{\mathcal{V}} \,.\, \vec{\nu} = \vec{u} \,.\, \vec{\nu} \qquad \text{on } \Gamma(t)\,, \tag{2.4c}$$

where $\gamma > 0$ is the surface tension coefficient and $\varkappa$ denotes the mean curvature of $\Gamma(t)$, i.e. the sum of the principal curvatures of $\Gamma(t)$, where we have adopted the sign convention that $\varkappa$ is negative where $\Omega_-(t)$ is locally convex. In particular, see e.g. [14], it holds that

$$\Delta_s\,\vec{\mathrm{id}} = \varkappa\,\vec{\nu} \qquad \text{on } \Gamma(t)\,, \tag{2.5}$$

where $\Delta_s = \nabla_s \,.\, \nabla_s$ is the Laplace–Beltrami operator on $\Gamma(t)$ with $\nabla_s \,.$ and ∇_s denoting surface divergence and surface gradient on $\Gamma(t)$, respectively. Moreover, as usual, $[\vec{u}]^+_- := \vec{u}_+ - \vec{u}_-$ and $[\underline{\underline{\sigma}}\,\vec{\nu}]^+_- := \underline{\underline{\sigma}}_+\,\vec{\nu} - \underline{\underline{\sigma}}_-\,\vec{\nu}$ denote the jumps in velocity and normal stress across the interface $\Gamma(t)$. Here and throughout, we employ the shorthand notation $\vec{g}_\pm := \vec{g}\,|_{\Omega_\pm(t)}$ for a function $\vec{g} : \Omega \times [0,T] \to \mathbb{R}^d$; and similarly for scalar and matrix-valued functions. To close the system we prescribe the initial data $\Gamma(0) = \Gamma_0$ and the boundary condition $\vec{u} = \vec{0}$ on $\partial\Omega$.

Therefore the total system can be rewritten as follows:

$$-2\mu\,\nabla \,.\, \underline{\underline{D}}(\vec{u}) + \nabla\, p = \vec{f} \qquad \text{in } \Omega_\pm(t)\,, \tag{2.6a}$$

$$\nabla \,.\, \vec{u} = 0 \qquad \text{in } \Omega_\pm(t)\,, \tag{2.6b}$$

$$\vec{u} = \vec{0} \qquad \text{on } \partial\Omega\,, \tag{2.6c}$$

$$[\vec{u}]^+_- = \vec{0} \qquad \text{on } \Gamma(t)\,, \tag{2.6d}$$

$$[2\mu\,\underline{\underline{D}}(\vec{u}) \,.\, \vec{\nu} - p\,\vec{\nu}]^+_- = -\gamma\,\varkappa\,\vec{\nu} \qquad \text{on } \Gamma(t)\,, \tag{2.6e}$$

$$(\vec{\mathcal{V}} - \vec{u}) \,.\, \vec{\nu} = 0 \qquad \text{on } \Gamma(t)\,, \tag{2.6f}$$

$$\Gamma(0) = \Gamma_0\,. \tag{2.6g}$$

2.2 Weak formulation

In order to obtain a weak formulation, we define the function spaces

$$\mathbb{U} := [H^1_0(\Omega)]^d\,, \qquad \mathbb{P} := L^2(\Omega) \qquad \text{and} \qquad \widehat{\mathbb{P}} := \{\eta \in \mathbb{P} : \int_\Omega \eta \,\mathrm{d}\mathcal{L}^d = 0\}\,,$$

and let $(\cdot,\cdot)$ and $\langle\cdot,\cdot\rangle_{\Gamma(t)}$ denote the L^2–inner products on Ω and $\Gamma(t)$, respectively. In addition, we let $\mathcal{L}^d$ and $\mathcal{H}^{d-1}$ denote the Lebesgue measure in $\mathbb{R}^d$ and the $(d-1)$-dimensional Hausdorff measure, respectively.

Multiplying (2.5) with a test function, and performing integration by parts, yields

$$\langle \varkappa\,\vec{\nu}, \vec{\eta}\rangle_{\Gamma(t)} + \left\langle \nabla_s\,\vec{\mathrm{id}}, \nabla_s\,\vec{\eta}\right\rangle_{\Gamma(t)} = 0 \quad \forall\ \vec{\eta} \in [H^1(\Gamma(t))]^d\,.$$

Moreover, on noting (2.2) and (2.4b), we have that

$$\begin{aligned}\int_{\Omega_+(t)\cup\Omega_-(t)} (\nabla \,.\, \underline{\underline{\sigma}}) \,.\, \vec{\xi}\,\mathrm{d}\mathcal{L}^d &= -\left(\underline{\underline{\sigma}}, \nabla\,\vec{\xi}\right) - \left\langle [\underline{\underline{\sigma}}\,\vec{\nu}]^+_-, \vec{\xi}\right\rangle_{\Gamma(t)} \\ &= \left(p, \nabla \,.\, \vec{\xi}\right) - 2\left(\mu\,\underline{\underline{D}}(\vec{u}), \underline{\underline{D}}(\vec{\xi})\right) + \gamma\left\langle \varkappa\,\vec{\nu}, \vec{\xi}\right\rangle_{\Gamma(t)}\end{aligned}$$

for all $\vec{\xi} \in [H^1_0(\Omega)]^d$. Hence a possible weak formulation of (2.6a–g) is given as follows. Given $\Gamma(0) = \Gamma_0$, for almost all $t \in (0,T)$ find $\Gamma(t)$ and $(\vec{u}, p, \varkappa)$

$\in \mathbb{U} \times \widehat{\mathbb{P}} \times H^1(\Gamma(t))$ such that

$$2\left(\mu\,\underline{\underline{D}}(\vec{u}),\underline{\underline{D}}(\vec{\xi})\right) - \left(p, \nabla\,.\,\vec{\xi}\right) - \gamma\,\left\langle \varkappa\,\vec{\nu},\vec{\xi}\right\rangle_{\Gamma(t)} = \left(\vec{f},\vec{\xi}\right) \quad \forall\ \vec{\xi} \in \mathbb{U}\,, \tag{2.7a}$$

$$(\nabla\,.\,\vec{u},\varphi) = 0 \quad \forall\ \varphi \in \widehat{\mathbb{P}}\,, \tag{2.7b}$$

$$\left\langle \vec{\mathcal{V}} - \vec{u}, \chi\,\vec{\nu}\right\rangle_{\Gamma(t)} = 0 \quad \forall\ \chi \in H^1(\Gamma(t))\,, \tag{2.7c}$$

$$\langle \varkappa\,\vec{\nu},\vec{\eta}\rangle_{\Gamma(t)} + \left\langle \nabla_s\,\vec{\mathrm{id}}, \nabla_s\,\vec{\eta}\right\rangle_{\Gamma(t)} = 0 \quad \forall\ \vec{\eta} \in [H^1(\Gamma(t))]^d \tag{2.7d}$$

holds for almost all times $t \in (0,T]$. Here we have observed that if $p \in \mathbb{P}$ is part of a solution to (2.6a–g), then so is $p + c$ for an arbitrary $c \in \mathbb{R}$.

2.3 Energy bound and volume conservation

It is straightforward to show an a priori energy bound and a volume conservation property for the system (2.7a–d). For the former, we recall from e.g. [14, Lemma 2.1] that

$$\frac{\mathrm{d}}{\mathrm{d}t}\,\mathcal{H}^{d-1}(\Gamma(t)) = -\left\langle \varkappa, \vec{\mathcal{V}}\,.\,\vec{\nu}\right\rangle_{\Gamma(t)}. \tag{2.8}$$

Hence, on choosing $\vec{\xi} = \vec{u}$ in (2.7a), and noting (2.7b,c), we obtain that

$$\gamma\,\frac{\mathrm{d}}{\mathrm{d}t}\,\mathcal{H}^{d-1}(\Gamma(t)) = -\gamma\,\langle \varkappa\,\vec{\nu},\vec{u}\rangle_{\Gamma(t)} = -2\left(\mu\,\underline{\underline{D}}(\vec{u}),\underline{\underline{D}}(\vec{u})\right) + \left(\vec{f},\vec{u}\right), \tag{2.9}$$

and so in the absence of outer forces, the interfacial energy is monotonically decreasing.

In order to show the volume conservation property, we recall from e.g. [14, Lemma 2.1] that

$$\frac{\mathrm{d}}{\mathrm{d}t}\mathcal{L}^d(\Omega_-(t)) = \left\langle \vec{\mathcal{V}},\vec{\nu}\right\rangle_{\Gamma(t)}. \tag{2.10}$$

Hence it follows immediately from the incompressibility condition (2.7b) and (2.7c) that

$$\frac{\mathrm{d}}{\mathrm{d}t}\mathcal{L}^d(\Omega_-(t)) = \langle \vec{u},\vec{\nu}\rangle_{\Gamma(t)} = \int_{\Omega_-(t)} \nabla\,.\,\vec{u}\,\mathrm{d}\mathcal{L}^d = 0\,. \tag{2.11}$$

It will be our aim to introduce a fitted finite element approximation for two-phase Stokes flow that satisfies discrete analogous of (2.9) and (2.11).

3 Numerical method

3.1 Finite element approximation

We consider the partitioning $0 = t_0 < t_1 < \ldots < t_{M-1} < t_M = T$ of $[0,T]$ into possibly variable time steps $\tau_m := t_{m+1} - t_m$, $m = 0, \ldots, M-1$. Moreover, let $\mathcal{T}^m$, $\forall m \geq 0$, be a regular partitioning of the domain Ω into disjoint open simplices o_j^m, $j = 1, \ldots, J_\Omega^m$. On $\mathcal{T}^m$ we define the finite element spaces

$$S_k^m := \{\chi \in C(\overline{\Omega}) : \chi|_{o^m} \in \mathcal{P}_k(o^m) \;\forall\; o^m \in \mathcal{T}^m\} \subset H^1(\Omega), \quad k \in \mathbb{N}\,,$$

where $\mathcal{P}_k(o^m)$ denotes the space of polynomials of degree k on o^m. Moreover, S_0^m is the space of piecewise constant functions on $\mathcal{T}^m$.

Let $\mathbb{U}^m \subset \mathbb{U}$ and $\mathbb{P}^m \subset \mathbb{P}$ be the finite element spaces we use for the approximation of velocity and pressure, and let $\widehat{\mathbb{P}}^m := \mathbb{P}^m \cap \widehat{\mathbb{P}}$. The spaces $(\mathbb{U}^m, \mathbb{P}^m)$ satisfy the LBB inf-sup condition if there exists a constant $C_0 \in \mathbb{R}_{>0}$, independent of $\mathcal{T}^m$, such that

$$\inf_{\varphi \in \widehat{\mathbb{P}}^m} \sup_{\vec{\xi} \in \mathbb{U}^m} \frac{(\varphi, \nabla \cdot \vec{\xi})}{\|\varphi\|_0 \, \|\vec{\xi}\|_1} \geq C_0 > 0\,, \tag{3.1}$$

see [21, p. 114]. Here $\|\cdot\|_0 := (\cdot,\cdot)^{\frac{1}{2}}$ and $\|\cdot\|_1 := \|\cdot\|_0 + \|\nabla \cdot\|_0$ denote the L^2–norm and the H^1–norm on Ω, respectively. Throughout this paper, we will assume that $S_0^m \subset \mathbb{P}^m$. Then, for $d = 2$, possible pairs $(\mathbb{U}^m, \mathbb{P}^m)$ that satisfy (3.1) are P2–P0 and P2–(P1+P0), i.e. we set $\mathbb{U}^m = [S_2^m]^d \cap \mathbb{U}$ and either $\mathbb{P}^m = S_0^m$ or $S_1^m + S_0^m$. We note that the choice P2–(P1+P0) requires the weak constraint that all simplices have a vertex in Ω, see [12]. For $d = 3$, pairs of spaces that satisfy $S_0^m \subset \mathbb{P}^m$ and (3.1) are the P3–(P2+P0) element, see [12], or stabilized spaces such as P1$^{\text{face bubble}}$–P0, see [11, Remark 8.7.1], which is also called the SMALL element.

In this paper we consider a fitted finite element approximation for the evolution of the interface $\Gamma(t)$. Let $\Gamma^m \subset \mathbb{R}^d$ be a $(d-1)$-dimensional polyhedral surface approximating the closed surface $\Gamma(t_m)$, $m = 0, \ldots, M$. Let Ω_+^m denote the exterior of Γ^m and let Ω_-^m be the interior of Γ^m, where we assume that Γ^m has no self-intersections. Then $\Omega = \Omega_-^m \cup \Gamma^m \cup \Omega_+^m$, and the fitted nature of our method implies that

$$\overline{\Omega_+^m} = \bigcup_{o \in \mathcal{T}_+^m} \overline{o} \quad \text{and} \quad \overline{\Omega_-^m} = \bigcup_{o \in \mathcal{T}_-^m} \overline{o}\,, \tag{3.2}$$

where $\mathcal{T}^m = \mathcal{T}_+^m \cup \mathcal{T}_-^m$ and $\mathcal{T}_+^m \cap \mathcal{T}_-^m = \emptyset$. Let $\vec{\nu}^m$ denote the piecewise constant unit normal to Γ^m such that $\vec{\nu}^m$ points into Ω_+^m.

In order to define the parametric finite element spaces on Γ^m, we assume that $\Gamma^m = \bigcup_{j=1}^{J_\Gamma} \overline{\sigma_j^m}$, where $\{\sigma_j^m\}_{j=1}^{J_\Gamma}$ is a family of mutually disjoint open $(d-1)$-simplices with vertices $\{\vec{q}_k^m\}_{k=1}^{K_\Gamma}$. Following the notation in [7], see also [5], we define $\underline{V}(\Gamma^m) :=$

$\{\vec{\chi} \in [C(\Gamma^m)]^d : \vec{\chi}\,|_{\sigma_j^m} \in \mathcal{P}_1(\sigma_j^m), j = 1, \ldots, J_\Gamma\} =: [W(\Gamma^m)]^d$, where $W(\Gamma^m) \subset H^1(\Gamma^m)$ is the space of scalar continuous piecewise linear functions on Γ^m, with $\{\chi_k^m\}_{k=1}^{K_\Gamma}$ denoting the standard basis of $W(\Gamma^m)$.

Moreover we define $\pi^m : C(\Gamma^m) \to W(\Gamma^m)$ the standard interpolation operator at the nodes $\{\vec{q}_k^m\}_{k=1}^{K_\Gamma}$, and similarly $\vec{\pi}^m : [C(\Gamma^m)]^d \to \underline{V}(\Gamma^m)$. Throughout this paper, we parameterize the new surface Γ^{m+1} over Γ^m using a parameterization $\vec{X}^{m+1} \in \underline{V}(\Gamma^m)$, so that $\Gamma^{m+1} = \vec{X}^{m+1}(\Gamma^m)$. Before we can state our numerical method, we need to introduce a mass lumped inner product on Γ^m, that is crucial for the desired tangential motion of vertices on Γ^m. This induced tangential motion will lead to good interface mesh properties. If $v, w \in L^\infty(\Gamma^m)$ are piecewise continuous, with possible jumps across the edges of $\{\sigma_j^m\}_{j=1}^{J_\Gamma}$, we define the mass lumped inner product $\langle \cdot, \cdot \rangle_{\Gamma^m}^h$ as

$$\langle v, w \rangle_{\Gamma^m}^h := \tfrac{1}{d} \sum_{j=1}^{J_\Gamma} \mathcal{H}^{d-1}(\sigma_j^m) \sum_{k=1}^{d} (v\,w)((\vec{q}_{j_k}^m)^-), \tag{3.3}$$

where $\{\vec{q}_{j_k}^m\}_{k=1}^d$ are the vertices of σ_j^m, and where we define the limit $v((\vec{q}_{j_k}^m)^-) := \lim_{\sigma_j^m \ni \vec{p} \to \vec{q}_{j_k}^m} v(\vec{p})$. We naturally extend (3.3) to vector valued functions. Similarly, we let $\langle \cdot, \cdot \rangle_{\Gamma^m}$ denote the standard L^2–inner product on Γ^m.

Then our finite element approximation, which is based on the variational formulation (2.7a–d), is given as follows. Let Γ^0 be an approximation to $\Gamma(0)$. For $m = 0, \ldots, M-1$, find $(\vec{U}^{m+1}, P^{m+1}, \vec{X}^{m+1}, \kappa^{m+1}) \in \mathbb{U}^m \times \widehat{\mathbb{P}}^m \times \underline{V}(\Gamma^m) \times W(\Gamma^m)$ such that

$$2\left(\mu^m\, \underline{\underline{D}}(\vec{U}^{m+1}), \underline{\underline{D}}(\vec{\xi})\right) - \left(P^{m+1}, \nabla \,.\, \vec{\xi}\right) - \gamma \left\langle \kappa^{m+1}\, \vec{\nu}^m, \vec{\xi} \right\rangle_{\Gamma^m} = \left(\vec{f}^{m+1}, \vec{\xi}\right) \qquad \forall\, \vec{\xi} \in \mathbb{U}^m\,, \tag{3.4a}$$

$$\left(\nabla \,.\, \vec{U}^{m+1}, \varphi\right) = 0 \quad \forall\, \varphi \in \widehat{\mathbb{P}}^m\,, \tag{3.4b}$$

$$\left\langle \frac{\vec{X}^{m+1} - \mathrm{i}\vec{\mathrm{d}}}{\tau_m}, \chi\, \vec{\nu}^m \right\rangle_{\Gamma^m}^h - \left\langle \vec{U}^{m+1}, \chi\, \vec{\nu}^m \right\rangle_{\Gamma^m} = 0 \quad \forall\, \chi \in W(\Gamma^m)\,, \tag{3.4c}$$

$$\left\langle \kappa^{m+1}\, \vec{\nu}^m, \vec{\eta} \right\rangle_{\Gamma^m}^h + \left\langle \nabla_s \vec{X}^{m+1}, \nabla_s \vec{\eta} \right\rangle_{\Gamma^m} = 0 \quad \forall\, \vec{\eta} \in \underline{V}(\Gamma^m) \tag{3.4d}$$

and set $\Gamma^{m+1} = \vec{X}^{m+1}(\Gamma^m)$. Here we have defined $\vec{f}^{m+1}(\cdot) := \vec{I}_2^m\, \vec{f}(\cdot, t_{m+1})$, where $\vec{I}_2^m$ is the standard interpolation operator onto $[S_2^m]^d$ and $\mu^m = \mu_+\, \mathcal{X}_{\Omega_+^m} + \mu_-\, \mathcal{X}_{\Omega_-^m} \in S_0^m$. We observe that (3.4a–d) is a linear scheme in that it leads to a coupled linear system of equations for the unknowns $(\vec{U}^{m+1}, P^{m+1}, \vec{X}^{m+1}, \kappa^{m+1})$ at each time level. We also note that the scheme (3.4a–d), in the context of an unfitted finite element approximation, has been considered in [7]. In particular, most of the theoretical results presented in the following are a direct consequence of the results in [7].

3.2 Existence and uniqueness of a discrete solution

Theorem 1. *Let $m \in \{0, \ldots, M-1\}$ and let $(\mathbb{U}^m, \mathbb{P}^m)$ satisfy the LBB condition (3.1). Then there exists a unique solution $(\vec{U}^{m+1}, P^{m+1}, \vec{X}^{m+1}, \kappa^{m+1}) \in \mathbb{U}^m \times \widehat{\mathbb{P}}^m \times \underline{V}(\Gamma^m) \times W(\Gamma^m)$ to (3.4a–d).*

Proof. As the system (3.4a–d) is linear, existence follows from uniqueness. In order to establish the latter, we consider the system: Find $(\vec{U}, P, \vec{X}, \kappa) \in \mathbb{U}^m \times \widehat{\mathbb{P}}^m \times \underline{V}(\Gamma^m) \times W(\Gamma^m)$ such that

$$2\left(\mu^m \underline{\underline{D}}(\vec{U}), \underline{\underline{D}}(\vec{\xi})\right) - \left(P, \nabla \,.\, \vec{\xi}\right) - \gamma \left\langle \kappa\, \vec{\nu}^m, \vec{\xi} \right\rangle_{\Gamma^m} = 0 \quad \forall\, \vec{\xi} \in \mathbb{U}^m\,, \tag{3.5a}$$

$$\left(\nabla \,.\, \vec{U}, \varphi\right) = 0 \quad \forall\, \varphi \in \widehat{\mathbb{P}}^m\,, \tag{3.5b}$$

$$\left\langle \vec{X}, \chi\, \vec{\nu}^m \right\rangle^h_{\Gamma^m} - \tau_m \left\langle \vec{U}, \chi\, \vec{\nu}^m \right\rangle_{\Gamma^m} = 0 \quad \forall\, \chi \in W(\Gamma^m)\,, \tag{3.5c}$$

$$\langle \kappa\, \vec{\nu}^m, \vec{\eta} \rangle^h_{\Gamma^m} + \left\langle \nabla_s \vec{X}, \nabla_s \vec{\eta} \right\rangle_{\Gamma^m} = 0 \quad \forall\, \vec{\eta} \in \underline{V}(\Gamma^m)\,. \tag{3.5d}$$

Choosing $\vec{\xi} = \vec{U}$ in (3.5a), $\varphi = P$ in (3.5b), $\chi = \gamma\,\kappa$ in (3.5c) and $\vec{\eta} = \gamma\, \vec{X}$ in (3.5d) yields that

$$2\,\tau_m \left(\mu^m \underline{\underline{D}}(\vec{U}), \underline{\underline{D}}(\vec{U})\right) + \gamma \left\langle \nabla_s \vec{X}, \nabla_s \vec{X} \right\rangle_{\Gamma^m} = 0\,. \tag{3.6}$$

It immediately follows from (3.6) and a Korn's inequality that $\vec{U} = \vec{0}$. In addition, it holds that $\vec{X}$ is equal to a constant on Γ^m, which satisfies, on recalling (3.5c) and $\vec{U} = \vec{0}$, that

$$\left\langle \vec{X}, \chi\, \vec{\nu}^m \right\rangle^h_{\Gamma^m} = 0 \quad \forall\, \chi \in W(\Gamma^m)\,. \tag{3.7}$$

It was shown in [5, Proof of Theorem 2.1] that if Γ^m has no self-intersections, then (3.7) immediately yields that $\vec{X} = \vec{0}$. As $\Gamma^m = \partial\Omega^m_-$ is the boundary of an open domain, we always assume that it does not self-intersect, and hence we obtain that $\vec{X} = \vec{0}$. This means that (3.5d) reduces to

$$\langle \kappa\, \vec{\nu}^m, \vec{\eta} \rangle^h_{\Gamma^m} = 0 \quad \forall\, \vec{\eta} \in \underline{V}(\Gamma^m)\,. \tag{3.8}$$

Let $\vec{\omega}^m \in \underline{V}(\Gamma^m)$ be the mass-lumped L^2–projection of $\vec{\nu}^m$ onto $\underline{V}(\Gamma^m)$, i.e. $\langle \vec{\omega}^m, \vec{\varphi} \rangle^h_{\Gamma^m} = \langle \vec{\nu}^m, \vec{\varphi} \rangle^h_{\Gamma^m} = \langle \vec{\nu}^m, \vec{\varphi} \rangle_{\Gamma^m}$ for all $\vec{\varphi} \in \underline{V}(\Gamma^m)$. It is easy to see that $\vec{\omega}^m(\vec{q}^m_k) \neq \vec{0}$ for all $k = 1, \ldots, K_\Gamma$, because Γ^m does not self-intersect. Then it follows from choosing $\vec{\eta} = \vec{\omega}^m$ in (3.8) that

$$0 = \langle \kappa\, \vec{\nu}^m, \vec{\omega}^m \rangle^h_{\Gamma^m} = \langle \vec{\nu}^m, \vec{\pi}^m[\kappa\, \vec{\omega}^m] \rangle_{\Gamma^m} = \langle \vec{\omega}^m, \vec{\pi}^m[\kappa\, \vec{\omega}^m] \rangle^h_{\Gamma^m} = \left\langle \kappa, |\vec{\omega}^m|^2 \right\rangle^h_{\Gamma^m}\,,$$

and so $\kappa = 0 \in W(\Gamma^m)$. Finally, it follows from (3.5a) with $\vec{U} = \vec{0}$ and $\kappa = 0$, on recalling (3.1), that $P = 0$. Hence there exists a unique solution $(\vec{U}^{m+1}, P^{m+1}, \vec{X}^{m+1}, \kappa^{m+1}) \in \mathbb{U}^m \times \widehat{\mathbb{P}}^m \times \underline{V}(\Gamma^m) \times W(\Gamma^m)$ to (3.4a–d). ∎

We note that if $(\mathbb{U}^m, \mathbb{P}^m)$ does not satisfy the LBB condition (3.1), then existence and uniqueness of the solution $(\vec{U}^{m+1}, \vec{X}^{m+1}, \kappa^{m+1})$ to a reduced system, where the pressure P^{m+1} is eliminated, can be shown. See [7, Theorem 1] for more details.

3.3 Stability

We now demonstrate that the scheme (3.4a–d) satisfies an energy estimate, which corresponds to the bound (2.9) in the continuous case. In particular, we obtain an unconditional stability result for our scheme.

Theorem 2. *Let $m \in \{0, \dots, M-1\}$ and let $(\vec{U}^{m+1}, P^{m+1}, \vec{X}^{m+1}, \kappa^{m+1}) \in \mathbb{U}^m \times \widehat{\mathbb{P}}^m \times \underline{V}(\Gamma^m) \times W(\Gamma^m)$ be a solution to* (3.4a–d)*. Then*

$$\gamma\, \mathcal{H}^{d-1}(\Gamma^{m+1}) + 2\,\tau_m \left(\mu^m\, \underline{\underline{D}}(\vec{U}^{m+1}), \underline{\underline{D}}(\vec{U}^{m+1})\right) \leq \gamma\, \mathcal{H}^{d-1}(\Gamma^m) + \tau_m \left(\vec{f}^{m+1}, \vec{U}^{m+1}\right). \tag{3.9}$$

In addition, let $\{t_k\}_{k=0}^M$ be an arbitrary partitioning of $[0,T]$. Then it holds that

$$\gamma\, \mathcal{H}^{d-1}(\Gamma^{m+1}) + 2 \sum_{k=0}^{m} \tau_k \left(\mu^k\, \underline{\underline{D}}(\vec{U}^{k+1}), \underline{\underline{D}}(\vec{U}^{k+1})\right) \leq \gamma\, \mathcal{H}^{d-1}(\Gamma^0) + \sum_{k=0}^{m} \tau_k \left(\vec{f}^{k+1}, \vec{U}^{k+1}\right) \tag{3.10}$$

for $m = 0, \dots, M-1$.

Proof. The desired results follow from choosing $\vec{\xi} = \vec{U}^{m+1} \in \mathbb{U}^m$ in (3.4a), $\varphi = P^{m+1} \in \widehat{\mathbb{P}}^m$ in (3.4b), $\chi = \gamma\, \kappa^{m+1}$ in (3.4c) and $\vec{\eta} = \gamma\, (\vec{X}^{m+1} - \vec{\mathrm{id}}\,|_{\Gamma^m})$ in (3.4d). See [7, Proof of Theorem 2] for more details. ☐

3.4 Discrete stationary solutions

If the solution $(\vec{U}^{m+1}, P^{m+1}, \vec{X}^{m+1}, \kappa^{m+1})$ to (3.4a–d) is such that the interface has not moved, $\Gamma^{m+1} = \Gamma^m$, then it holds that

$$\exists\, \zeta \in W(\Gamma^m) \;:\quad \langle \zeta\, \vec{\nu}^m, \vec{\eta} \rangle_{\Gamma^m}^h + \left\langle \nabla_s\, \vec{\mathrm{id}}, \nabla_s\, \vec{\eta} \right\rangle_{\Gamma^m} = 0 \quad \forall\, \vec{\eta} \in \underline{V}(\Gamma^m)\,. \tag{3.11}$$

We recall from [4, Remark 2.4] that (3.11) in the case $d = 2$ implies that Γ^m is equidistributed, with the possible exception of elements σ_j^m that are locally parallel to each other; see also [6, Theorem 2.2]. Moreover, we recall from [5, §4.1] that surfaces $\Gamma^m \subset \mathbb{R}^3$ that satisfy (3.11) are called conformal polyhedral surfaces.

Next we can prove that discrete stationary solution exist for our scheme.

Theorem 3. *Let $(\mathbb{U}^m, \mathbb{P}^m)$ satisfy the LBB condition* (3.1) *and let $S_0^m \subset \mathbb{P}^m$. Let $\vec{f}^{m+1} = \vec{0}$. Moreover, let Γ^m be a polyhedral surface with constant discrete mean curvature, i.e. there exists a constant $\overline{\kappa} \in \mathbb{R}$ such that*

$$\overline{\kappa}\, \langle \vec{\nu}^m, \vec{\eta} \rangle_{\Gamma^m} + \left\langle \nabla_s\, \vec{\mathrm{id}}, \nabla_s\, \vec{\eta} \right\rangle_{\Gamma^m} = 0 \quad \forall\, \vec{\eta} \in \underline{V}(\Gamma^m)\,. \tag{3.12}$$

Then Γ^m *satisfies* (3.11) *and*

$$(\vec{U}^{m+1}, P^{m+1}, \vec{X}^{m+1}, \kappa^{m+1}) = (\vec{0}, -\gamma\,\overline{\kappa}\left[\mathcal{X}_{\Omega^m_-} - \frac{\mathcal{L}^d(\Omega^m_-)}{\mathcal{L}^d(\Omega)}\right], \vec{\mathrm{id}}\,|_{\Gamma^m}, \overline{\kappa}) \tag{3.13}$$

is the unique solution to (3.4a–d).

Proof. It immediately follows from (3.12) that (3.11) holds. We now show that the solution stated in (3.13) solves (3.4a–d). Since $\mathcal{X}_{\Omega^m_-} \in \mathbb{P}^m$, we have that $P^{m+1} \in \widehat{\mathbb{P}}^m$, and so (3.13) is admissible. Clearly, the three equations (3.4b), (3.4c) and (3.4d) hold trivially. In order to show that (3.4a) holds, we observe that the divergence theorem implies that

$$-\gamma\left\langle \kappa^{m+1}\,\vec{\nu}^m, \vec{\xi}\right\rangle_{\Gamma^m} = -\gamma\,\overline{\kappa}\left\langle \vec{\nu}^m, \vec{\xi}\right\rangle_{\Gamma^m} = -\gamma\,\overline{\kappa}\left(\nabla\,.\,\vec{\xi}, \mathcal{X}_{\Omega^m_-}\right) = \left(\nabla\,.\,\vec{\xi}, P^{m+1}\right)$$

for all $\vec{\xi} \in \mathbb{U}^m$, where we have observed that P^{m+1} differs from $-\gamma\,\overline{\kappa}\,\mathcal{X}_{\Omega^m_-}$ only by a constant. Hence (3.4a) also holds, and so (3.13) is the unique solution to (3.4a–d) □

We remark that in practice we do observe the solution (3.13) for approximations of stationary spherical bubble solutions, see §4.1 and §4.5 for details.

3.5 Semidiscrete scheme

We briefly investigate a semidiscrete variant of the scheme (3.4a–d) in order to highlight two additional important properties of the scheme: a good tangential distribution of mesh points, and good volume conservation.

Let $(\Gamma^h(t))_{t\in[0,T]}$ be a family of polyhedral surfaces, with outer normal $\vec{\nu}^h(t)$. We also define the piecewise linear finite element spaces $W(\Gamma^h(t))$ and $\underline{V}(\Gamma^h(t))$, with $\{\chi^h_k(\cdot,t)\}_{k=1}^{K_\Gamma}$ denoting the standard basis of the former. Hence $\chi^h_k(\vec{q}^h_l(t),t) = \delta_{kl}$ for all $k,l \in \{1,\ldots,K_\Gamma\}$ and $t \in [0,T]$, where $\{\vec{q}^h_k(t)\}_{k=1}^{K_\Gamma}$ are the vertices of $\Gamma^h(t)$. Similarly to (2.1), we can then define the discrete velocity

$$\vec{\mathcal{V}}^h(\vec{z},t) := \sum_{k=1}^{K_\Gamma}\left[\frac{\mathrm{d}}{\mathrm{d}t}\,\vec{q}^h_k(t)\right]\chi^h_k(\vec{z},t) \in \underline{V}(\Gamma^h(t))\,,$$

see e.g. [8, (3.3)]. For $t \in [0,T]$, let $\mathcal{T}^h(t)$ be a regular partitioning of Ω into disjoint open simplices and define the finite element spaces $S^h_k(t)$, $\mathbb{U}^h(t)$ and $\mathbb{P}^h(t)$ similarly to S^m_k, $\mathbb{U}^m$ and $\mathbb{P}^m$, with the corresponding interpolation operators I^h_k and discrete approximations $\mu^h(t) \in S^h_0(t)$. Here we recall that we assume $S^h_0(t) \subset \mathbb{P}^h(t)$. Then,

given $\Gamma^h(0)$, for $t \in (0,T]$ find $\Gamma^h(t)$ and $(\vec{U}^h(t), P^h(t), \vec{\mathcal{V}}^h(t), \kappa^h(t)) \in \mathbb{U}^h(t) \times \widehat{\mathbb{P}}^h(t) \times \underline{V}(\Gamma^h(t)) \times W(\Gamma^h(t))$ such that

$$2\left(\mu^h\, \underline{\underline{D}}(\vec{U}^h), \underline{\underline{D}}(\vec{\xi})\right) - \left(P^h, \nabla\,.\,\vec{\xi}\right) - \gamma\, \left\langle \kappa^h\, \vec{\nu}^h, \vec{\xi} \right\rangle_{\Gamma^h(t)} = \left(\vec{f}^h, \vec{\xi}\right) \forall\ \vec{\xi} \in \mathbb{U}^h(t)\,, \tag{3.14a}$$

$$\left(\nabla\,.\,\vec{U}^h, \varphi\right) = 0 \quad \forall\ \varphi \in \widehat{\mathbb{P}}^h(t)\,, \tag{3.14b}$$

$$\left\langle \vec{\mathcal{V}}^h, \chi\, \vec{\nu}^h \right\rangle^h_{\Gamma^h(t)} - \left\langle \vec{U}^h, \chi\, \vec{\nu}^h \right\rangle_{\Gamma^h(t)} = 0 \quad \forall\ \chi \in W(\Gamma^h(t))\,, \tag{3.14c}$$

$$\left\langle \kappa^h\, \vec{\nu}^h, \vec{\eta} \right\rangle^h_{\Gamma^h(t)} + \left\langle \nabla_s\, \vec{\mathrm{id}}, \nabla_s\, \vec{\eta} \right\rangle_{\Gamma^h(t)} = 0 \quad \forall\ \vec{\eta} \in \underline{V}(\Gamma^h(t))\,, \tag{3.14d}$$

where $\vec{f}^h := \vec{I}^h_2\, \vec{f}(t)$.

First of all we note that a solution $\Gamma^h(t)$ to (3.14a–d) clearly satisfies (3.11), with Γ^m replaced by $\Gamma^h(t)$. This means that in 2d the polygonal curve $\Gamma^h(t)$ is equidistributed, and asymptotically this property is inherited by our fully discrete scheme (3.4a–d); see e.g. Figure 6 below. In 3d the property (3.11) means that $\Gamma^h(t)$ is a conformal polyhedral surface, which implies that the mesh quality is good. Once again, we observe in practice that the fully discrete solutions to (3.4a–d) also exhibit nice meshes, without coalescence or other mesh defects occurring.

Secondly, we can show that solutions to (3.14a–d) satisfy a discrete analogue of (2.11). To see this, choose $\chi = 1$ in (3.14c) and $\varphi = (\mathcal{X}_{\Omega^h_-(t)} - \frac{\mathcal{L}^d(\Omega^h_-(t))}{\mathcal{L}^d(\Omega)}) \in \widehat{\mathbb{P}}^h(t)$ in (3.14b), to obtain

$$\begin{aligned}\frac{\mathrm{d}}{\mathrm{d}t}\mathcal{L}^d(\Omega^h_-(t)) &= \left\langle \vec{\mathcal{V}}^h, \vec{\nu}^h \right\rangle_{\Gamma^h(t)} = \left\langle \vec{\mathcal{V}}^h, \vec{\nu}^h \right\rangle^h_{\Gamma^h(t)} = \left\langle \vec{U}^h, \vec{\nu}^h \right\rangle_{\Gamma^h(t)} \\ &= \int_{\Omega^h_-(t)} \nabla\,.\,\vec{U}^h\ \mathrm{d}\mathcal{L}^d = 0\,.\end{aligned}$$

Hence solution to (3.14a–d) conserve the enclosed volume. Once again, the fully discrete scheme (3.4a–d) inherits this property in the sense that in our simulations the volumes are always well maintained.

3.6 Solution method

As is standard practice for the solution of linear systems arising from discretizations of (Navier–)Stokes equations, we avoid the complications of the constrained pressure space $\widehat{\mathbb{P}}^m$ in practice by considering an overdetermined linear system with $\mathbb{P}^m$ instead. In a post-processing step the computed pressure is then projected into the space of zero mean functions. The linear system (3.4a–d), with $\widehat{\mathbb{P}}^m$ replaced by $\mathbb{P}^m$, can be formulated as:

Find $(\vec{U}^{m+1}, P^{m+1}, \kappa^{m+1}, \delta\vec{X}^{m+1}) \in (\mathbb{R}^d)^{K_{\mathbb{U}}^m} \times \mathbb{R}^{K_{\mathbb{P}}^m} \times \mathbb{R}^{K_\Gamma} \times (\mathbb{R}^d)^{K_\Gamma}$, where $\vec{X}^{m+1} = \vec{X}^m + \delta\vec{X}^{m+1}$, such that

$$\begin{pmatrix} \vec{B}_\Omega & \vec{C}_\Omega & -\gamma\,\vec{N}_{\Gamma,\Omega} & 0 \\ \vec{C}_\Omega^T & 0 & 0 & 0 \\ \vec{N}_{\Gamma,\Omega}^T & 0 & 0 & -\frac{1}{\tau_m}\,\vec{N}_\Gamma^T \\ 0 & 0 & \vec{N}_\Gamma & \vec{A}_\Gamma \end{pmatrix} \begin{pmatrix} \vec{U}^{m+1} \\ P^{m+1} \\ \kappa^{m+1} \\ \delta\vec{X}^{m+1} \end{pmatrix} = \begin{pmatrix} \vec{c} \\ 0 \\ 0 \\ -\vec{A}_\Gamma\,\vec{X}^m \end{pmatrix}, \tag{3.15}$$

where $(\vec{U}^{m+1}, P^{m+1}, \kappa^{m+1}, \delta\vec{X}^{m+1})$ here denote the coefficients of these finite element functions with respect to the standard bases of $\mathbb{U}^m$, $\mathbb{P}^m$, $W(\Gamma^m)$ and $\underline{V}(\Gamma^m)$, respectively. Moreover, $\vec{X}^m$ denotes the coefficients of $\vec{\mathrm{id}}\,|_{\Gamma^m}$ with respect to the basis of $\underline{V}(\Gamma^m)$. The definitions of the matrices and vectors in (3.15) directly follow from (3.4a–d).

Note that for the submatrices we have used the convention that the subscripts refer to the test and trial domains, respectively. A single subscript is used where the two domains are the same.

For the solution of (3.15) we use a Schur complement approach that eliminates $(\kappa^{m+1}, \delta\vec{X}^{m+1})$ from (3.15), and then use an iterative solver for the remaining system in $(\vec{U}^{m+1}, P^{m+1})$. This approach has the advantage that for the reduced system well-known solution methods for finite element discretizations for standard (Navier–)Stokes discretizations may be employed. The desired Schur complement can be obtained as follows. Let

$$\Xi_\Gamma := \begin{pmatrix} 0 & -\frac{1}{\tau_m}\,\vec{N}_\Gamma^T \\ \vec{N}_\Gamma & \vec{A}_\Gamma \end{pmatrix}. \tag{3.16}$$

Then (3.15) can be reduced to

$$\begin{pmatrix} \vec{B}_\Omega + \gamma\,(\vec{N}_{\Gamma,\Omega}\ 0)\,\Xi_\Gamma^{-1} \begin{pmatrix} \vec{N}_{\Gamma,\Omega}^T \\ 0 \end{pmatrix} & \vec{C}_\Omega \\ \vec{C}_\Omega^T & 0 \end{pmatrix} \begin{pmatrix} \vec{U}^{m+1} \\ P^{m+1} \end{pmatrix} = \begin{pmatrix} \vec{c} - \gamma\,(\vec{N}_{\Gamma,\Omega}\ 0)\,\Xi_\Gamma^{-1} \begin{pmatrix} 0 \\ \vec{A}_\Gamma\,\vec{X}^m \end{pmatrix} \\ 0 \end{pmatrix} \tag{3.17a}$$

and

$$\begin{pmatrix} \kappa^{m+1} \\ \delta\vec{X}^{m+1} \end{pmatrix} = \Xi_\Gamma^{-1} \begin{pmatrix} -\vec{N}_{\Gamma,\Omega}^T\,\vec{U}^{m+1} \\ -\vec{A}_\Gamma\,\vec{X}^m \end{pmatrix}. \tag{3.17b}$$

For the solution of (3.17a) we employ a preconditioned GMRES iterative solver, where for the inverse Ξ_Γ^{-1} we employ a sparse $L\,U$ decomposition, which we obtain with the help of the sparse factorization package UMFPACK, see [13]. Having obtained $(\vec{U}^{m+1}, P^{m+1})$ from (3.17a), we solve (3.17b) for $(\kappa^{m+1}, \delta\vec{X}^{m+1})$.

Remark 4. *With a view towards some numerical test cases in Section 4, we also allow for an inhomogeneous Dirichlet boundary condition $\vec{g}$ on $\partial\Omega$. In this case the*

linear system is suitably adjusted. For example, in place of (3.4b)*, with* $\widehat{\mathbb{P}}^m$ *replaced by* $\mathbb{P}^m$*, we require*

$$\left(\nabla \,.\, \vec{U}^{m+1}, \varphi\right) = \frac{(\varphi, 1)}{\mathcal{L}^d(\Omega)} \int_{\partial\Omega} (\vec{I}_2^m \, \vec{g}) \,.\, \vec{\mathrm{n}} \, \mathrm{d}\mathcal{H}^{d-1} \quad \forall \, \varphi \in \mathbb{P}^m \,. \tag{3.18}$$

3.7 Mesh generation and smoothing

Given the initial polyhedral surface Γ^0, we create a triangulation $\mathcal{T}^0$ of Ω that is fitted to Γ^0 with the help of the package `Gmsh`, see [20]. Then, for $m \geq 0$, having computed the new interface Γ^{m+1}, we would like to obtain a bulk triangulation $\mathcal{T}^{m+1}$ that is fitted to Γ^{m+1}, and ideally is close to $\mathcal{T}^m$. This is to avoid unnecessary overhead from remeshing the domain Ω completely.

To this end, we perform the following smoothing step on $\mathcal{T}^m$, which is inspired by the method proposed in [17], see also [19]. Having obtained $\delta\vec{X}^{m+1}$ from the solution of (3.15), we solve the linear elasticity problem: Find a displacement $\vec{\psi} \in [H^1(\Omega)]^d$ such that

$$\nabla \,.\, \underline{\underline{S}} = \vec{0} \qquad \text{in } \Omega_\pm^m \,, \tag{3.19a}$$

$$\vec{\psi} = \delta\vec{X} \qquad \text{on } \Gamma^m \,, \tag{3.19b}$$

$$\vec{\psi} \,.\, \vec{\mathrm{n}} = 0 \qquad \text{on } \partial\Omega \,, \tag{3.19c}$$

where the stress tensor $\underline{\underline{S}}$ is defined as

$$\underline{\underline{S}} = 2\,\underline{\underline{D}}(\vec{\psi}) + (\nabla \,.\, \vec{\psi})\,\underline{\underline{\mathrm{id}}} \tag{3.20}$$

and where $\vec{\mathrm{n}}$ in (3.19c) is the outer unit normal to Ω on $\partial\Omega$. In practice we approximate (3.19a–c) with piecewise linear elements and solve the resulting system of linear equations with the UMPFACK package, see [13]. The obtained discrete variant of $\vec{\psi}$, at every vertex of the current bulk grid $\mathcal{T}^m$, then represents the variation in their position that we compute in order to obtain $\mathcal{T}^{m+1}$.

Occasionally the deformation of the mesh becomes too large, for instance when the bubble making up the inner phase undergoes strong deformations, and so a complete remeshing of Ω becomes necessary. In order to detect the need for a complete remeshing, we define the criterion

$$\frac{\max_{o \in \mathcal{T}^{m+1}} (\mathcal{H}^d(o))}{\min_{o \in \mathcal{T}^{m+1}} (\mathcal{H}^d(o))} \geq C_r \geq 1, \tag{3.21}$$

where C_r is a fixed constant. Of course, if we choose $C_r = 1$, then a remeshing would be triggered after every time step.

We stress that in all our numerical simulations we never need to remesh the interface Γ^m itself. Hence the stability results from Theorem 2 hold throughout. Of course, a remeshing of Γ^m would mean that Theorem 2 is no longer valid.

4 Numerical results

We implemented the scheme (3.4a–d) with the help of the toolbox `DUNE`, see [10, 9], using the finite element module `DUNE-FEM`, see [15]. As grid manager we used `ALBERTA`, see [33]. The CPU times which we report are measured in seconds and correspond to a single thread computation on an Intel Xeon E5640 (2.67GHz) processor with 16 GB of main memory.

In order to test our method, and to allow comparisons with the unfitted finite element approximation in [7], we recall the following stationary and expanding spherical solutions from [7]. Let $\Gamma(t) = \{\vec{z} \in \mathbb{R}^d : |\vec{z}| = r(t)\}$ be a sphere of radius $r(t)$ and curvature $\kappa(t) = -\frac{d-1}{r(t)}$. Firstly, the stationary sphere where

$$r(t) = r(0)\,, \tag{4.1a}$$

together with

$$\vec{u}(\vec{z},t) = \vec{0}\,, \quad p(\vec{z},t) = -\gamma\kappa(0)\left[\mathcal{X}_{\Omega_-(0)} - \frac{\mathcal{L}^d(\Omega_-(0))}{\mathcal{L}^d(\Omega)}\right], \tag{4.1b}$$

is an exact solution to the problem (2.6a–g) on e.g. $\Omega = (-1,1)^d$. This solution is the continuous version of (3.13). Secondly, a nontrivial divergence free and radially symmetric solution $\vec{u}$ can be constructed on a domain that does not contain the origin. To this end, consider e.g. $\Omega = (-1,1)^d \setminus [-\frac{1}{3},\frac{1}{3}]^d$, and let $\alpha \geq 0$ be given. Then, the expanding sphere where

$$r(t) = ([r(0)]^d + \alpha\, t\, d)^{\frac{1}{d}}\,, \tag{4.2a}$$

together with

$$\vec{u}(\vec{z},t) = \alpha\,\frac{\vec{z}}{|\vec{z}|^d}\,, \quad p(\vec{z},t) = -\left(\gamma + 2\,\alpha\,\frac{\mu_+ - \mu_-}{r(t)^{d-1}}\right)\kappa(t)\,\left[\mathcal{X}_{\Omega_-(t)} - \frac{\mathcal{L}^d(\Omega_-(t))}{\mathcal{L}^d(\Omega)}\right], \tag{4.2b}$$

is an exact solution to the problem (2.6a–g) with the homogeneous right hand side in (2.6c) replaced by $\vec{g}$, where $\vec{g}(\vec{z}) = \alpha\,|\vec{z}|^{-d}\,\vec{z}$. We will refer to (4.1a,b) as the stationary bubble solution, and to (4.2a,b) as the expanding bubble solution.

In the following, unless otherwise stated, we choose the initial surface $\Gamma(0) = \{\vec{z} \in \mathbb{R}^d : |\vec{z}| = \frac{1}{2}\}$, the domain $\Omega = (-1,1)^d$ and we employ uniform time steps $\tau_m = \tau$, $m = 0,\ldots,M-1$.

Moreover, we define the errors

$$\|\Gamma^h - \Gamma\|_{L^\infty} := \max_{m=1,\ldots,M} \|\Gamma^m - \Gamma(t_m)\|_{L^\infty}\,, \tag{4.3}$$

where $\|\Gamma^m - \Gamma(t_m)\|_{L^\infty} := \max_{k=1,\ldots,K_\Gamma} \operatorname{dist}(\vec{q}_k^{\,m}, \Gamma(t_m))$,

$$\|\vec{U} - I_2^h\,\vec{u}\|_{L^2} := \left[\tau \sum_{m=1}^{M} \|\vec{U}^m - I_2^m\,\vec{u}(\cdot,t_m)\|^2_{L^2(\Omega)}\right]^{\frac{1}{2}}, \tag{4.4}$$

$$\|\vec{U} - I_2^h\,\vec{u}\|_{H^1} := \left[\tau \sum_{m=1}^{M} \|\vec{U}^m - I_2^m\,\vec{u}(\cdot,t_m)\|^2_{H^1(\Omega)}\right]^{\frac{1}{2}}, \tag{4.5}$$

and

$$\|P - p\|_{L^2} := \left[\tau \sum_{m=1}^{M} \|P^m - p(\cdot,t_m)\|^2_{L^2(\Omega)}\right]^{\frac{1}{2}}. \tag{4.6}$$

In (4.6) we employ a quadrature rule of degree k, with $k = 13$ in 2d and $k = 10$ in 3d, to compute the L^2–norms over Ω.

4.1 Convergence tests in 2d

For the true solution (4.1a,b) we choose $\mu = \gamma = 1$. Therefore, the solution reduces to $r(t) = \frac{1}{2}$, $\vec{u}(\cdot,t) = \vec{0}$ and $p(t) = 2\,\mathcal{X}_{\Omega_-(0)} - \frac{\pi}{8}$ for all $t \geq 0$. We approximate this stationary solution on nearly uniform meshes that feature $J_\Gamma = 2^i$, $i = 4,\ldots,7$, uniform interface elements and $J_\Omega^0 = 224$, 1076, 4240, 17194 bulk elements, respectively. We show the initial mesh for $J_\Gamma = 32$ in Figure 2. In addition, we use a

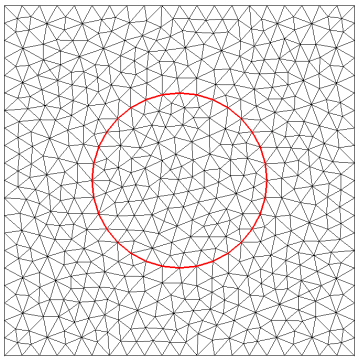

Figure 2: Initial mesh for the 2d stationary bubble problem with $J_\Gamma = 32$ interface elements.

uniform time step size $\tau = 10^{-2}$. We compute the discrete solutions to this stationary problem over the time interval $[0,1]$, and report on the errors for the P2–P0 and P2–(P1+P0) elements in Tables 1 and 2, respectively. We can clearly see that the stationary nature of the true solution (4.1a,b) is captured exactly by our numerical

J_Γ	$\|\Gamma^h - \Gamma\|_{L^\infty}$	$\|\vec{U} - I_2^h\,\vec{u}\|_{L^2}$	$\|P - p\|_{L^2}$	EOC	CPU[s]
16	0	0	3.22254e-01	-	9
32	0	0	1.41195e-01	0.90	54
64	0	0	4.06438e-02	1.80	292
128	0	0	2.60448e-02	0.64	1443

Table 1: ($\mu = \gamma = 1$) Stationary bubble problem on $(-1,1)^2$ over the time interval $[0,1]$ for the P2–P0 element.

J_Γ	$\|\Gamma^h - \Gamma\|_{L^\infty}$	$\|\vec{U} - I_2^h\,\vec{u}\|_{L^2}$	$\|P - p\|_{L^2}$	EOC	CPU[s]
16	0	0	3.22254e-01	-	13
32	0	0	1.41195e-01	0.90	44
64	0	0	4.06438e-02	1.80	203
128	0	0	2.60448e-02	0.64	2151

Table 2: ($\mu = \gamma = 1$) Stationary bubble problem on $(-1,1)^2$ over the time interval $[0,1]$ for the P2–(P1+P0) element.

method, see also Figure 3 for a visualization of the discrete pressure in the case $J_\Gamma = 32$. This is not surprising given the result of Theorem 3, and the fact that we use an equidistributed approximation Γ^0, which means that (3.12) is satisfied. Of course, since the discrete solution is stationary, neither smoothing nor remeshing is performed for the simulations in Tables 1 and 2. We also observe that the error for the two approximations with the P2–P0 and the P2–(P1+P0) element, respectively, produce identical errors. Again, that is to be expected, since the solution (3.13) is such that $P^{m+1} \in S_0^m$, and so the additional degrees of freedom in the space S_1^m are not utilized by the pressure approximation.

For the expanding bubble test, we fix $\Omega = (-1,1)^2 \setminus [-\frac{1}{3},\frac{1}{3}]^2$ and we choose the parameters $\alpha = 0.15$ and $\mu_+ = 10\,\mu_- = \gamma = 1$ for the true solution (4.2a,b). Here we consider two different bulk mesh strategies. Either we use a nearly uniform mesh, as shown on the left of Figure 4, or an adaptive mesh that uses a finer resolution close to the interface, see the example mesh on the right hand side of Figure 4.

Details on the discretization parameters for the nearly uniform meshes are given in Table 3. Here we explicitly state the final number of bulk elements, J_Ω^M, only in the case $C_r = 1$, recall (3.21), i.e. when the bulk is remeshed after every time step. Of course, when only smoothing is employed, then the number of bulk mesh elements is invariant, and so $J_\Omega^M = J_\Omega^0$. We report on the error for the P2–P0 element, when only mesh smoothings are applied, in Table 4. Due to the expanding motion of the interface, we observe that over time bulk mesh elements strongly deform. This leads to large CPU times and additional approximation errors. In particular, the strong mesh deformations for the finest run, with $J_\Omega^0 = J_\Omega^M = 15212$,

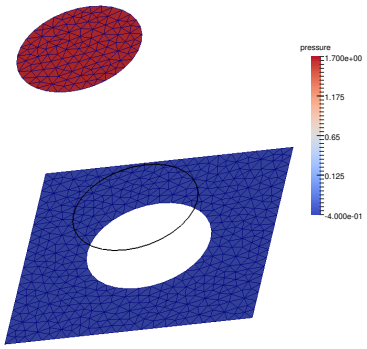

Figure 3: ($\mu = \gamma = 1$) Pressure of the 2d stationary bubble at time $t = 1$ for the P2–P0 element.

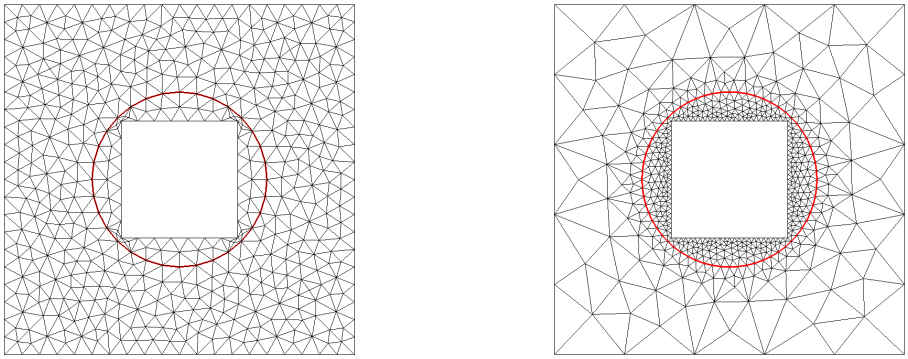

Uniform mesh with $J_\Gamma = 32$ | Adaptive mesh with $J_\Gamma = 64$

Figure 4: Initial meshes for the expanding bubble problem.

J_Γ	J_Ω^0	τ	J_Ω^M for $C_r = 1$
16	212	$1.6 \cdot 10^{-2}$	120
32	988	$4 \cdot 10^{-3}$	452
64	3776	10^{-3}	1864
128	15212	$2.5 \cdot 10^{-4}$	7272

Table 3: Discretization parameters for the 2d expanding bubble problem, uniform meshes.

J_Γ	$\|\Gamma^h - \Gamma\|_{L^\infty}$	$\|\vec{U} - I_2^h\,\vec{u}\|_{L^2}$	EOC	$\|\vec{U} - I_2^h\,\vec{u}\|_{H^1}$	$\|P - p\|_{L^2}$	EOC	CPU[s]
16	6.17082e-03	8.84787e-04	-	2.50884e-02	4.16967e-01	-	5
32	1.51156e-03	3.41220e-04	1.04	1.17669e-02	2.29638e-01	0.65	119
64	3.69491e-04	8.66470e-05	1.98	5.82977e-03	1.05959e-01	1.12	2121
128	9.20954e-05	5.90688e-05	0.55	6.42798e-03	3.15158e-02	1.75	37494

Table 4: ($\mu_+ = 10\,\mu_- = \gamma = 1, \alpha = 0.15$) Expanding bubble problem on $(-1,1)^2 \setminus [-\frac{1}{3},\frac{1}{3}]^2$ over the time interval $[0,1]$ for the P2–P0 element, no remeshing and uniform mesh.

J_Γ	$\|\Gamma^h - \Gamma\|_{L^\infty}$	$\|\vec{U} - I_2^h\,\vec{u}\|_{L^2}$	EOC	$\|\vec{U} - I_2^h\,\vec{u}\|_{H^1}$	$\|P - p\|_{L^2}$	EOC	CPU[s]
16	5.96720e-03	5.50015e-04	-	1.59994e-02	4.43219e-01	-	17
32	1.46664e-03	1.05702e-04	1.80	5.25702e-03	2.14651e-01	0.79	142
64	3.65441e-04	1.48680e-05	2.83	1.50700e-03	8.09626e-02	1.41	1598
128	9.12537e-05	1.80890e-06	3.04	3.59193e-04	3.69595e-02	1.13	26254

Table 5: ($\mu_+ = 10\,\mu_- = \gamma = 1, \alpha = 0.15$) Expanding bubble problem on $(-1,1)^2 \setminus [-\frac{1}{3},\frac{1}{3}]^2$ over the time interval $[0,1]$ for the P2–P0 element, with remeshing at every time step and uniform mesh.

leads to a breakdown of the convergence rate for the L^2-velocity error, and an actual increase in the H^1-velocity error. Hence, as a comparison, we show the errors for the same element, when the bulk mesh is remeshed after every time step, in Table 5.

We observe a dramatic improvement in the CPU times, and a significant reduction in the error quantities. In particular, there is no deterioration of the observed convergence rates. That is why for the P2–(P1+P0) element we only consider the case $C_r = 1$, see Table 6, i.e. only a simulation with remeshing at every time step. Comparing the errors in Tables 5 and 6 we note slightly larger CPU times for the latter, which is not surprising, and slightly larger error quantities. It is for this reason that for all the remaining numerical computations we will only consider the

J_Γ	$\|\Gamma^h - \Gamma\|_{L^\infty}$	$\|\vec{U} - I_2^h\,\vec{u}\|_{L^2}$	EOC	$\|\vec{U} - I_2^h\,\vec{u}\|_{H^1}$	$\|P - p\|_{L^2}$	EOC	CPU[s]
16	5.96973e-03	9.14482e-04	-	2.64868e-02	4.44352e-01	-	16
32	1.47267e-03	2.41367e-04	1.45	1.03904e-02	2.14909e-01	0.79	168
64	3.65603e-04	2.33325e-05	3.37	2.02177e-03	8.11567e-02	1.40	2177
128	9.12677e-05	2.42999e-06	3.26	4.31899e-04	3.69626e-02	1.13	29120

Table 6: ($\mu_+ = 10\,\mu_- = \gamma = 1, \alpha = 0.15$) Expanding bubble problem on $(-1,1)^2 \setminus [-\frac{1}{3},\frac{1}{3}]^2$ over the time interval $[0,1]$ for the P2–(P1+P0) element, with remeshing at every time step and uniform mesh.

J_Γ	J_Ω^0	τ	J_Ω^M
32	584	$6.4 \cdot 10^{-2}$	234
64	1020	$1.6 \cdot 10^{-2}$	564
128	2506	$4 \cdot 10^{-3}$	1226
256	7460	10^{-3}	3866

Table 7: Discretization parameters for the 2d expanding bubble problem, adaptive meshes.

P2–P0 element.

The evolution of the discrete pressure solution in the case $J_\Gamma = 32$, for the run with $C_r = 1$, can be seen in Figure 5. Here we note that the discontinuous

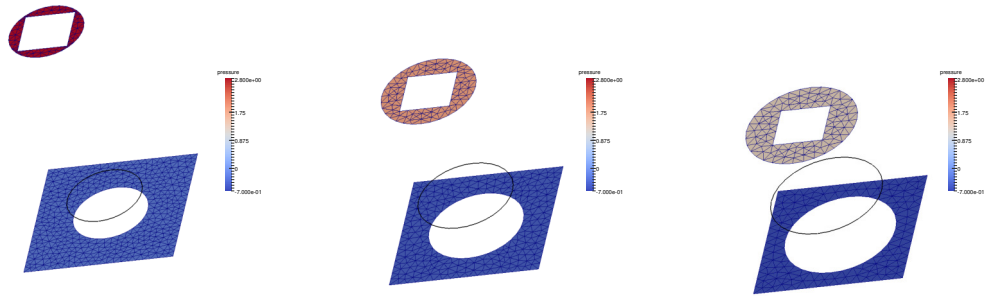

$t = 0$ $t = 0.5$ $t = 1$

Figure 5: ($\mu_+ = 10\,\mu_- = \gamma = 1, \alpha = 0.15$) Pressure evolution of the 2d expanding bubble for the P2–P0 element, uniform mesh.

jump in the pressure at the interface is captured very well, with no oscillations being present. This is a significant improvement on the oscillations observed in the discrete pressures for the unfitted finite element approximation from [7], see e.g. Figure 6 in that paper.

Finally, we would also like to investigate the effect of using adaptive bulk meshes, that are refined close to the interface. An example mesh is shown on the right hand side of Figure 4, and we list our employed discretization parameters in Table 7. The observed errors for our numerical approximation are shown in Table 8. Comparing the error quantities in Tables 5 and 8 we note that there appears to be no advantage in using a highly refined mesh near the moving interface.

4.2 Equidistribution property in 2d

We now demonstrate the remarkable equidistribution property of our method showing that the circular, equidistributed numerical steady state solution is recovered by

J_Γ	$\|\Gamma^h - \Gamma\|_{L^\infty}$	$\|\vec{U} - I_2^h \vec{u}\|_{L^2}$	EOC	$\|\vec{U} - I_2^h \vec{u}\|_{H^1}$	$\|P - p\|_{L^2}$	EOC	CPU[s]
32	3.92051e-03	6.54288e-04	-	1.43866e-02	5.58359e-01	-	5
64	9.96712e-04	3.70951e-04	0.62	1.09825e-02	2.94547e-01	0.70	25
128	2.60197e-04	2.88781e-04	0.36	9.81011e-03	1.51576e-01	0.96	238
256	6.05795e-05	6.98183e-05	2.05	3.87054e-03	6.32656e-02	1.26	2624

Table 8: ($\mu_+ = 10\,\mu_- = \gamma = 1, \alpha = 0.15$) Expanding bubble problem on $(-1,1)^2 \setminus [-\frac{1}{3},\frac{1}{3}]^2$ over the time interval $[0,1]$ for the P2–P0 element, with remeshing at every time step and adaptive mesh.

our method even if we choose a very nonuniform initial interface Γ^0. In particular, for the presented numerical simulation, we take Γ^0 to be a very nonuniform approximation of a unit circle, where we represent the upper half of the circle by a single vertex, while the lower half resembles a semicircle. In total we use $J_\Gamma = 32$ elements for Γ^0 and we start with a very nonuniform bulk mesh with $J_\Omega^0 = 670$ elements. Of course, the initial bulk mesh has to respect the nonuniform approximation of the interface, and so is very nonuniform itself. However, we see from the evolution in Figure 6 that as the interface gets closer and closer to an equidistributed approximation of a circle, the bulk mesh also becomes more uniform. For the presented simulation we used the physical parameters $\mu = \gamma = 1$. The uniform time step size is chosen as $\tau = 10^{-4}$ and we set $C_r = 3$, recall (3.21).

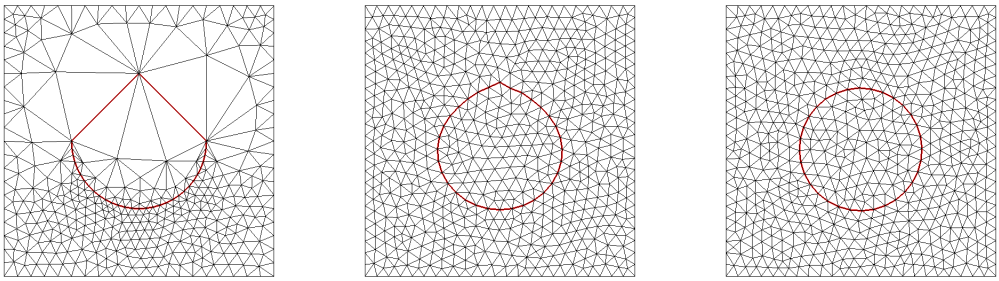

$t = 0$ $t = 1$ $t = 5$

Figure 6: ($\mu = \gamma = 1$) Mesh evolution of a nonuniform circle formed by $J_\Gamma = 32$ elements. Here we use the P2–P0 element, and let $C_r = 3$.

4.3 Energy decay and area conservation in 2d

In Figure 7 we show the pressure evolution for a simulation that starts with an initial ellipse, with major and minor axes of 1.6 and 0.75. We use the parameters $\mu = \gamma = 1$, $\tau = 10^{-2}$ and $T = 10$. The initial interface is discretized with $J_\Gamma = 40$

surface elements, and the initial bulk mesh has $J_\Omega^0 = 1112$ elements. We employ the P2–P0 element and use the remeshing parameter $C_r = 3$ during the evolution. Figure 8 shows the evolution of the relative inner area $\frac{\mathcal{L}^2(\Omega_-^m)}{\mathcal{L}^2(\Omega_-^0)}$ and the evolution of the interface energy $\gamma\,\mathcal{H}^1(\Gamma^m)$. The graphs show that the inner area is nearly conserved, and that the interface energy is monotonically decreasing.

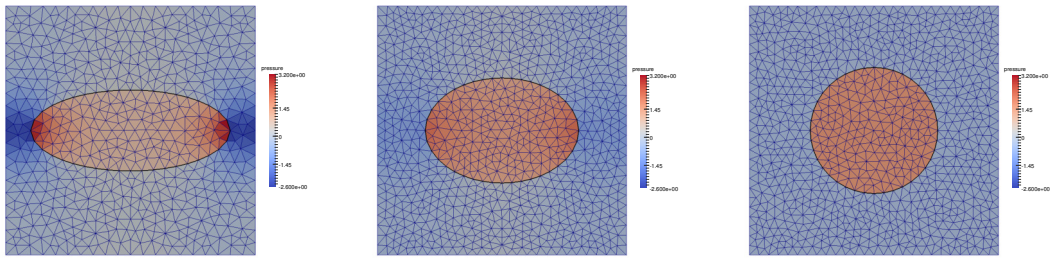

$t = 10^{-5}$ $t = 2.5$ $t = 10$

Figure 7: ($\mu = \gamma = 1$) Pressure evolution of an ellipse that evolves towards a circle. Here we use the P2–P0 element, and let $C_r = 3$.

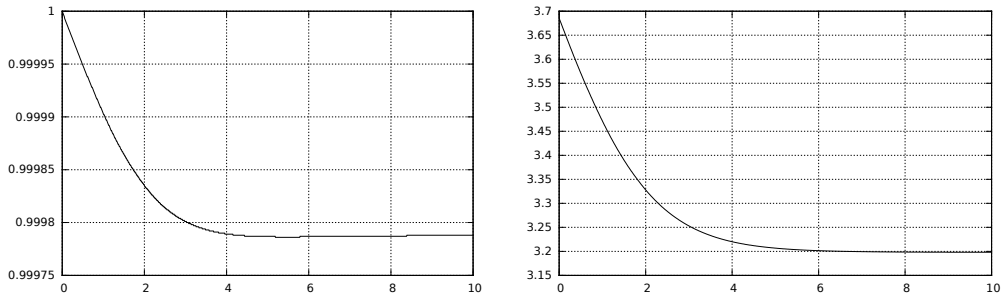

$\frac{\mathcal{L}^2(\Omega_-^m)}{\mathcal{L}^2(\Omega_-^0)}$ $\gamma\,\mathcal{H}^1(\Gamma^m)$

Figure 8: Evolutions of the relative inner area and the interface energy for the simulation in Figure 7.

As a comparison, we show in Figure 9 the final snapshot of the same simulation when no remeshings are performed, i.e. we use $C_r = \infty$ in (3.21). We clearly see that due to the strong deformation of the interface, this leads to elongated elements in the inner and in the outer phase of the bulk finite element mesh.

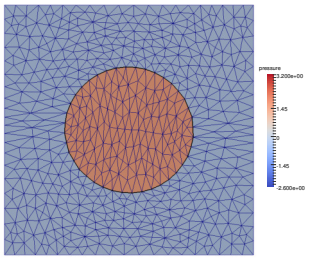

$t = 10$

Figure 9: ($\mu = \gamma = 1$) Final pressure solution for a simulation as in Figure 7, when no remeshings are performed.

4.4 Shear flow experiment in 2d

As the final 2d numerical simulation we present a shear flow experiment. Here we prescribe the inhomogeneous Dirichlet boundary condition

$$\vec{g}(\vec{z}) = (z_2, 0)^T \quad \text{on } \partial\Omega\,,$$

and we use the parameters $\mu = 1$, $\gamma = 3$, $\tau = 10^{-2}$ and $T = 5$. The initial interface is discretized with $J_\Gamma = 64$ surface elements, and the initial bulk mesh has $J_\Omega^0 = 4240$ elements. In Figure 10 we show the evolution of the discrete pressures for a simulation with $C_r = 3$ for the P2–P0 element, while the velocities are visualized in Figure 11.

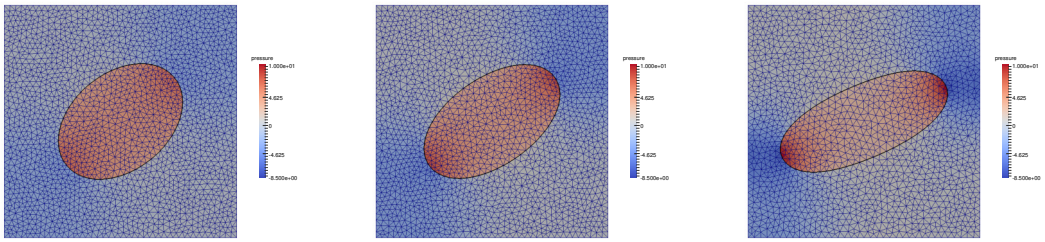

$t = 0.5$ $\qquad$ $t = 1$ $\qquad$ $t = 5$

Figure 10: ($\mu = 1, \gamma = 3$) Pressure evolution for the 2d shear flow with $C_r = 3$ for the P2–P0 element, uniform mesh.

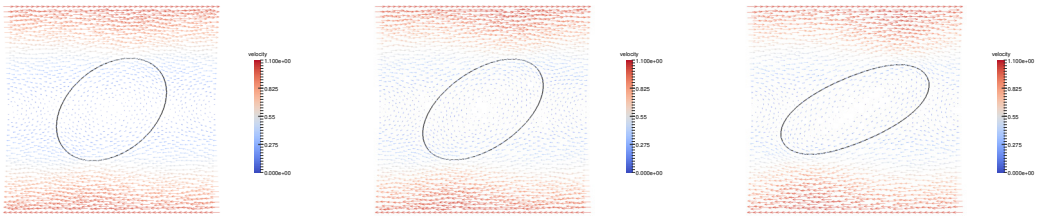

$t = 0.5$ $t = 1$ $t = 5$

Figure 11: ($\mu = 1, \gamma = 3$) Velocity vector field for the 2d shear flow with $C_r = 3$ for the P2–P0 element, uniform mesh.

4.5 Convergence test in 3d

Similarly to §4.1, we perform the following convergence test for a stationary spherical bubble in 3d. Let $\mu = \gamma = 1$. Then the true solution (4.1a,b) reduces to $r(t) = \frac{1}{2}$, $\vec{u}(\cdot, t) = \vec{0}$ and $p(t) = 4\,\mathcal{X}_{\Omega_-(0)} - \frac{\pi}{12}$ for all $t \geq 0$. We approximate this stationary solution on nearly uniform meshes that feature $J_\Gamma = 32$, 220 and 596 interface elements, and $J^0_\Omega = 408$, 3590 and 20473 bulk elements, respectively. Here, in contrast to the situation in 2d, we are not able to define Γ^0 such that the vertices of Γ^0 lie on $\Gamma(0)$ and such that (3.12) is satisfied. As we would like to demonstrate the ability of our method to recover the discrete stationary solution (3.13) also in 3d, we choose the initial interface Γ^0 such that (3.12) holds, at the expense of a nonzero initial error $\|\Gamma^0 - \Gamma(0)\|_{L^\infty}$, recall (4.3). We obtain such an initial triangulation with the help of the numerical scheme from [5] for surface diffusion, which is a gradient flow for surface area that maintains the enclosed volume. See e.g. [5, Fig. 11] for an evolution towards a polyhedral approximation of a sphere that satisfies (3.12), and hence also (3.11). We report the errors for the P2–P0 element in Table 9, while Table 10 shows the same errors for the P2–(P1+P0) element. Here we note that, as yet, for the pairs P2–P0 and P2–(P1+P0) there exist no proofs in the literature that the LBB condition (3.1) holds, see e.g. the discussion in [11, Remark 8.4.3]. However, in practice we encountered no problems when using these spaces, and our iterative solver always converged to a solution of the scheme (3.4a–d). For both sets of simulations we use the uniform time step size $\tau = 10^{-2}$.

We note that we again recover the discrete stationary solutions (3.13). Here this leads to a nonzero error in the position of the discrete interface, because the vertices of the initial interface Γ^0 do not lie on $\Gamma(0)$.

J_Γ	$\|\Gamma^h - \Gamma\|_{L^\infty}$	$\|\vec{U} - I_2^h\,\vec{u}\|_{L^2}$	$\|P - p\|_{L^2}$	EOC	CPU[s]
32	2.97986e-02	0	1.65555e-00	-	385
220	5.80971e-03	0	7.14269e-01	1.21	4699
596	2.42857e-03	0	3.58466e-01	0.99	51604

Table 9: ($\mu = \gamma = 1$) Stationary bubble problem on $(-1, 1)^3$ over the time interval $[0, 1]$ for the P2–P0 element.

J_Γ	$\|\Gamma^h - \Gamma\|_{L^\infty}$	$\|\vec{U} - I_2^h\,\vec{u}\|_{L^2}$	$\|P - p\|_{L^2}$	EOC	CPU[s]
32	2.97986e-02	0	1.65749e-00	-	568
220	5.80971e-03	0	7.15353e-01	1.21	9174
596	2.42857e-03	0	3.59181e-01	0.99	121110

Table 10: ($\mu = \gamma = 1$) Stationary bubble problem on $(-1, 1)^3$ over the time interval $[0, 1]$ for the P2–(P1+P0) element.

4.6 Shear flow experiment in 3d

Finally, we also report on a 3d shear flow experiment. The initial interface mesh has $J_\Gamma = 596$ elements, while the nearly uniform bulk mesh is made up of $J_\Omega^0 = 19641$ elements. We prescribe the inhomogeneous Dirichlet boundary condition

$$\vec{g}(\vec{z}) = (z_3, 0, 0)^T \quad \text{on } \partial\Omega\,,$$

and we use the parameters $\mu = 1$, $\gamma = 3$, $\tau = 10^{-2}$ and $T = 5$. In Figure 12 we show the evolution of the discrete interface for a simulation with $C_r = 3$ for the P2–P0 element, while the velocities are visualized in Figure 13.

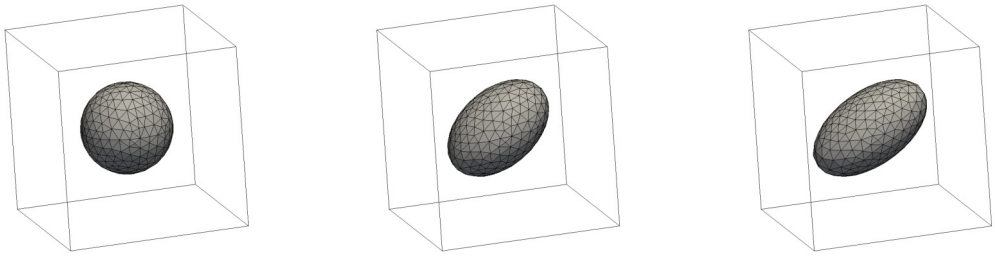

$t = 0$ $t = 1$ $t = 5$

Figure 12: ($\mu = 1, \gamma = 3$) Interface evolution for the 3d shear flow with $C_r = 3$ for the P2–P0 element, uniform mesh.

A plot of the relative inner volume over time is shown in Figure 14, where we again observe that our numerical method maintains the enclosed volume well.

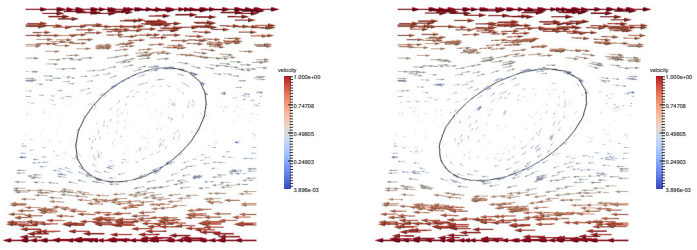

$t = 1$ $t = 5$

Figure 13: $(\mu = 1, \gamma = 3)$ Velocity vector field in the plane normal to $(0, 1, 0)^T$ and passing through the origin for the 3d shear flow with $C_r = 3$ for the P2–P0 element, uniform mesh.

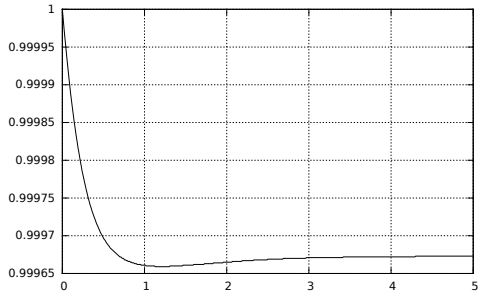

Figure 14: A plot of the relative inner volume $\frac{\mathcal{L}^3(\Omega_-^m)}{\mathcal{L}^3(\Omega_-^0)}$ over time for the simulation in Figure 12.

5 Conclusion

We have presented a novel fitted finite element approximation for two-phase Stokes flow. The method uses a piecewise linear approximation of the interface and employs standard velocity and pressure finite element spaces in the bulk.

The scheme is unconditionally stable and can capture simple stationary solutions exactly, which means that no spurious velocities appear. In addition, the discontinuous pressure jumps are captured well in general situations, and no pressure oscillations appear in practice.

Moreover, the numerical solutions exhibit good volume conservation properties and the quality of the interface mesh does not deteriorate in time.

References

[1] H. Abels, H. Garcke, and G. Grün, *Thermodynamically consistent, frame indifferent diffuse interface models for incompressible two-phase flows with different densities*, Math. Models Methods Appl. Sci., 22 (2012), p. 1150013.

[2] D. M. Anderson, G. B. McFadden, and A. A. Wheeler, *Diffuse-interface methods in fluid mechanics*, in Annual review of fluid mechanics, Vol. 30, Annual Reviews, Palo Alto, CA, 1998, pp. 139–165.

[3] E. Bänsch, *Finite element discretization of the Navier–Stokes equations with a free capillary surface*, Numer. Math., 88 (2001), pp. 203–235.

[4] J. W. Barrett, H. Garcke, and R. Nürnberg, *A parametric finite element method for fourth order geometric evolution equations*, J. Comput. Phys., 222 (2007), pp. 441–462.

[5] ——, *On the parametric finite element approximation of evolving hypersurfaces in* $\mathbb{R}^3$, J. Comput. Phys., 227 (2008), pp. 4281–4307.

[6] ——, *The approximation of planar curve evolutions by stable fully implicit finite element schemes that equidistribute*, Numer. Methods Partial Differential Equations, 27 (2011), pp. 1–30.

[7] ——, *Eliminating spurious velocities with a stable approximation of viscous incompressible two-phase Stokes flow*, Comput. Methods Appl. Mech. Engrg., 267 (2013), pp. 511–530.

[8] ——, *On the stable numerical approximation of two-phase flow with insoluble surfactant*, M2AN Math. Model. Numer. Anal., 49 (2015), pp. 421–458.

[9] P. Bastian, M. Blatt, A. Dedner, C. Engwer, R. Klöfkorn, R. Kornhuber, M. Ohlberger, and O. Sander, *A Generic Grid Interface for Parallel and Adaptive Scientific Computing. Part II: Implementation and Tests in DUNE*, Computing, 82 (2008), pp. 121–138.

[10] P. Bastian, M. Blatt, A. Dedner, C. Engwer, R. Klöfkorn, M. Ohlberger, and O. Sander, *A Generic Grid Interface for Parallel and Adaptive Scientific Computing. Part I: Abstract Framework*, Computing, 82 (2008), pp. 103–119.

[11] D. Boffi, F. Brezzi, and M. Fortin, *Mixed finite element methods and applications*, vol. 44 of Springer Series in Computational Mathematics, Springer, Heidelberg, 2013.

[12] D. Boffi, N. Cavallini, F. Gardini, and L. Gastaldi, *Local mass conservation of Stokes finite elements*, J. Sci. Comput., 52 (2012), pp. 383–400.

[13] T. A. Davis, *Algorithm 832: UMFPACK V4.3—an unsymmetric-pattern multifrontal method*, ACM Trans. Math. Software, 30 (2004), pp. 196–199.

[14] K. Deckelnick, G. Dziuk, and C. M. Elliott, *Computation of geometric partial differential equations and mean curvature flow*, Acta Numer., 14 (2005), pp. 139–232.

[15] A. Dedner, R. Klöfkorn, M. Nolte, and M. Ohlberger, *A Generic Interface for Parallel and Adaptive Scientific Computing: Abstraction Principles and the DUNE-FEM Module*, Computing, 90 (2010), pp. 165–196.

[16] X. Feng, *Fully discrete finite element approximations of the Navier–Stokes–Cahn–Hilliard diffuse interface model for two-phase fluid flows*, SIAM J. Numer. Anal., 44 (2006), pp. 1049–1072.

[17] S. Ganesan, *Finite element methods on moving meshes for free surface and interface flows*, PhD thesis, University Magdeburg, Magdeburg, Germany, 2006.

[18] S. Ganesan, G. Matthies, and L. Tobiska, *On spurious velocities in incompressible flow problems with interfaces*, Comput. Methods Appl. Mech. Engrg., 196 (2007), pp. 1193–1202.

[19] S. Ganesan and L. Tobiska, *An accurate finite element scheme with moving meshes for computing 3D-axisymmetric interface flows*, Internat. J. Numer. Methods Fluids, 57 (2008), pp. 119–138.

[20] C. Geuzaine and J.-F. Remacle, *Gmsh: A 3-D finite element mesh generator with built-in pre- and post-processing facilities*, Internat. J. Numer. Methods Engrg., 79 (2009), pp. 1309–1331.

[21] V. Girault and P.-A. Raviart, *Finite Element Methods for Navier–Stokes*, Springer-Verlag, Berlin, 1986.

[22] S. Gross and A. Reusken, *An extended pressure finite element space for two-phase incompressible flows with surface tension*, J. Comput. Phys., 224 (2007), pp. 40–58.

[23] G. Grün and F. Klingbeil, *Two-phase flow with mass density contrast: Stable schemes for a thermodynamic consistent and frame-indifferent diffuse-interface model*, J. Comput. Phys., 257 (2014), pp. 708–725.

[24] C. W. Hirt and B. D. Nichols, *Volume of fluid (VOF) method for the dynamics of free boundaries*, J. Comput. Phys., 39 (1981), pp. 201–225.

[25] P. C. Hohenberg and B. I. Halperin, *Theory of dynamic critical phenomena*, Rev. Mod. Phys., 49 (1977), pp. 435–479.

[26] D. Kay, V. Styles, and R. Welford, *Finite element approximation of a Cahn–Hilliard–Navier–Stokes system*, Interfaces Free Bound., 10 (2008), pp. 15–43.

[27] R. J. LeVeque and Z. Li, *Immersed interface methods for Stokes flow with elastic boundaries or surface tension*, SIAM J. Sci. Comput., 18 (1997), pp. 709–735.

[28] J. Lowengrub and L. Truskinovsky, *Quasi-incompressible Cahn-Hilliard fluids and topological transitions*, R. Soc. Lond. Proc. Ser. A Math. Phys. Eng. Sci., 454 (1998), pp. 2617–2654.

[29] S. Osher and R. Fedkiw, *Level Set Methods and Dynamic Implicit Surfaces*, vol. 153 of Applied Mathematical Sciences, Springer-Verlag, New York, 2003.

[30] C. S. Peskin, *The immersed boundary method*, Acta Numer., 11 (2002), pp. 479–517.

[31] S. Popinet, *An accurate adaptive solver for surface-tension-driven interfacial flows*, J. Comput. Phys., 228 (2009), pp. 5838–5866.

[32] Y. Renardy and M. Renardy, *PROST: a parabolic reconstruction of surface tension for the volume-of-fluid method*, J. Comput. Phys., 183 (2002), pp. 400–421.

[33] A. Schmidt and K. G. Siebert, *Design of Adaptive Finite Element Software: The Finite Element Toolbox ALBERTA*, vol. 42 of Lecture Notes in Computational Science and Engineering, Springer-Verlag, Berlin, 2005.

[34] J. A. Sethian, *Level Set Methods and Fast Marching Methods*, Cambridge University Press, Cambridge, 1999.

[35] M. Sussman, P. Semereka, and S. Osher, *A level set approach for computing solutions to incompressible two-phase flow*, J. Comput. Phys., 114 (1994), pp. 146–159.

[36] G. Tryggvason, B. Bunner, A. Esmaeeli, D. Juric, N. Al-Rawahi, W. Tauber, J. Han, S. Nas, and Y.-J. Jan, *A front-tracking method for the computations of multiphase flow*, J. Comput. Phys., 169 (2001), pp. 708–759.

[37] S. O. Unverdi and G. Tryggvason, *A front-tracking method for viscous, incompressible multi-fluid flows*, J. Comput. Phys., 100 (1992), pp. 25–37.